# Observation of Tunneling-Assisted Highly Forbidden Single-Photon Transitions in a $Ni_4$ Single-Molecule Magnet

Yiming Chen,[1,2] Mohammad D. Ashkezari,[1,*] Charles A. Collett,[1] Rafael A. Allão Cassaro,[3,†] Filippo Troiani,[4] Paul M. Lahti,[3] and Jonathan R. Friedman[1,‡]

[1]*Department of Physics and Astronomy, Amherst College, Amherst, Massachusetts 01002-5000, USA*
[2]*Department of Physics, University of Massachusetts, Amherst, Massachusetts 01003, USA*
[3]*Department of Chemistry, University of Massachusetts, Amherst, Massachusetts 01003, USA*
[4]*S3 Instituto Nanoscienze-CNR, I-41124 Modena, Italy*

(Received 1 August 2016; published 27 October 2016)

Forbidden transitions between energy levels typically involve violation of selection rules imposed by symmetry and/or conservation laws. A nanomagnet tunneling between up and down states violates angular momentum conservation because of broken rotational symmetry. Here we report observations of highly forbidden transitions between spin states in a $Ni_4$ single-molecule magnet in which a single photon can induce the spin to change by several times $\hbar$, nearly reversing the direction of the spin. These observations are understood as tunneling-assisted transitions that lift the standard $\Delta m = \pm 1$ selection rule for single-photon transitions. These transitions are observed at low applied fields, where tunneling is dominated by the molecule's intrinsic anisotropy and the field acts as a perturbation. Such transitions can be exploited to create macroscopic superposition states that are not typically accessible through single-photon $\Delta m = \pm 1$ transitions.

DOI: 10.1103/PhysRevLett.117.187202

There has been much recent attention to using spin systems as potential qubits [1–4]. Molecular nanomagnets are particularly attractive as spin qubits [4–12] because many of their properties can be chemically engineered. Single-molecule magnets (SMMs) are anisotropic molecular magnets, typically with a large total spin, for which the spin is impelled to point along a preferred axis, the "easy" axis [13]. They exhibit remarkable quantum dynamics including tunneling between different orientations [14] and quantum-phase interference [15]. Here we present evidence of highly forbidden transitions in the $Ni_4$ SMM where the transitions are enabled by tunneling, which lifts the requirement of spin angular momentum conservation. We observe transitions in which the absorption of a single photon permits a near reversal of the molecule's macrospin, grossly violating the standard $\Delta m = \pm 1$ selection rule. The quantum states that can be generated through these forbidden transitions are nonclassical, having a substantial "macroscopicity" by a standard measure. Our results imply that the forbidden transitions observed in this system (and similar molecules with strong anisotropy) can be exploited to create highly nonclassical states with single-photon transitions.

From a quantum coherence perspective, forbidden transitions have some distinct advantages: Since the matrix elements for these transitions are small, they tend to have long lifetimes. In addition, they can be less susceptible to magnetic-field fluctuations under certain circumstances, potentially leading to longer coherence times [3,12,16]. Forbidden transitions have been seen in SMMs with very strong tunneling produced by strongly broken symmetry [11,12,17]. In contrast, in our experiments the transitions are dominated by a modest intrinsic anisotropy with an applied field acting as a perturbation.

We studied the $S = 4$ complex $[Ni(hmp)(dmb)Cl]_4$ (hereafter $Ni_4$), shown in the inset of Fig. 1. The molecule's large ligands isolate the magnetic centers within a crystal from each other [18]. In addition, there are no solvate molecules in the crystal lattice and 99% (natural abundance) of Ni nuclei have spin $I = 0$. This SMM has been characterized by electron-spin resonance (ESR) spectroscopy [17,19–24], magnetization measurements [17,18,25] and heat capacity measurements [23,26,27]. $Ni_4$ can be well described as a single "giant spin" with the Hamiltonian [24]

$$\mathscr{H} = -DS_z^2 - AS_z^4 + C(S_+^4 + S_-^4) - \mu_B \vec{B} \cdot \mathbf{g} \cdot \vec{S}, \quad (1)$$

where $\mathbf{g}$ is the molecule's $g$ tensor, $D$ and $A$ are axial (diagonal) anisotropy parameters that define the easy $z$ axis and make the $m = \pm 4$ magnetic sublevels have the lowest energy, producing an energy barrier between those two orientations; $C$ is a transverse (off-diagonal) anisotropy parameter that affects the strength of tunneling through the barrier; and the magnetic field $\vec{B} = B(\sin\theta\cos\phi, \sin\theta\sin\phi, \cos\theta)$ produces a Zeeman interaction. The $z$ component of $\vec{B}$ changes the energies of the magnetic sublevels as illustrated in Fig. 1. When levels approach, the off-diagonal terms in Eq. (1) mix states of different $m$ values, giving rise to anticrossings. Like the transverse anisotropy, the transverse components of $\vec{B}$ are off-diagonal terms in Eq. (1). Since the off-diagonal terms do not commute

 

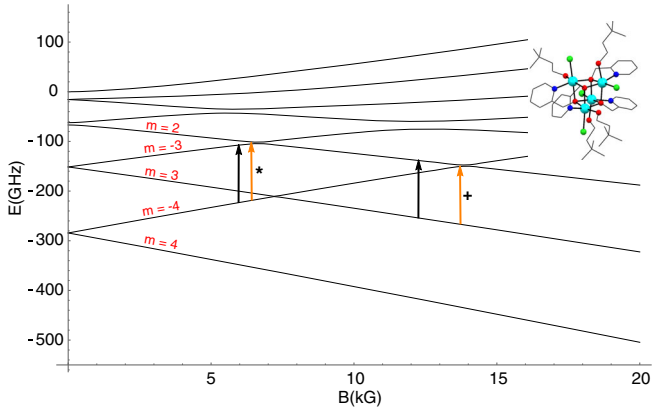


FIG. 1. Spin-state energy-level diagram for one conformational state ("black"—see below) of $Ni_4$. Energies of various levels are shown as a function of magnetic field, calculated by diagonalizing the molecule's spin Hamiltonian. The diagram illustrates the levels' behavior when $\theta = 30°$. Arrows indicate the major transitions observed in this study: Black = allowed, orange = forbidden. The two orange arrows are labeled with $\star$ and $+$, the designations used throughout this article. Inset: Molecular unit of $[Ni(hmp)(dmb)Cl]_4$ [18], where hmp is the anion of 2-hydroxymethylpyridine and dmb is 3,3-dimethyl-1-butanol. Color code: green, chloride; cyan, nickel(II); black, carbon; red, oxygen; blue, nitrogen. Hydrogens have been omitted for clarity.

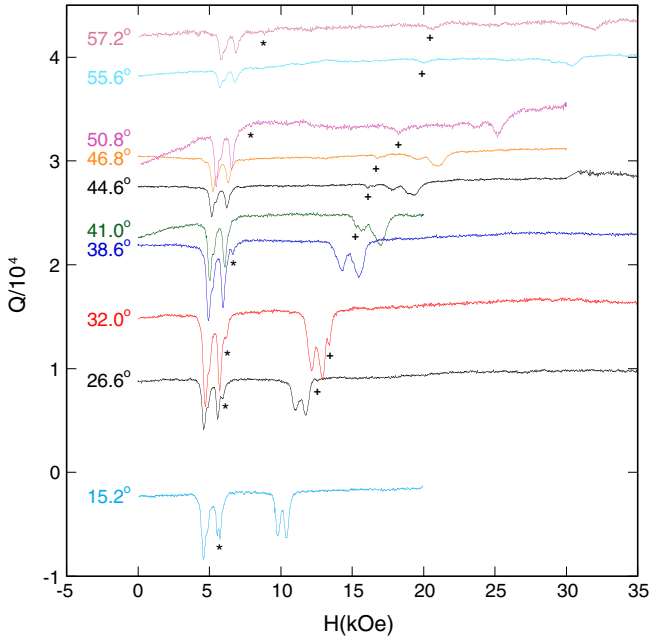


FIG. 2. Absorption ESR spectra at 1.8 K for several angles $\theta_H$. The spectrum for $\theta_{H,ref} = 26.6°$ shows actual $Q$ values. All other spectra have been shifted vertically by an amount proportional to $\theta_H - \theta_{H,ref}$. Spectra from three different crystals are combined in this figure. Each spectrum has been shifted slightly horizontally to account for inductive effects due to sweeping $H$ (see Ref. [28]).

with $S_z$, they are responsible for the observed tunneling phenomena in this and other SMMs [13,14]. The energy splitting at an anticrossing is dubbed the "tunnel splitting."

We performed reflection ESR spectroscopy using a 3D cylindrical resonant cavity with a $TE_{011}$ mode with resonant frequency ~115.54 GHz and a quality factor ($Q$) of ~10 000. A static magnetic field $\vec{H}$ was applied along the axis of the cavity. A single crystal of $Ni_4$ (synthesized using published procedures [25]) was mounted on the bottom of the cavity at a position where the rf field was perpendicular to the static field. The easy axis of the crystal was manually tilted at various angles ($\theta_H$) relative to $\vec{H}$. We measured the reflected power as a function of frequency and extracted the resonance frequency and $Q$ value of the cavity at each field [28].

Figure 2 shows ESR spectra ($Q$ vs $H$) at 1.8 K for a single crystal of $Ni_4$ at multiple values of $\theta_H$, the angle between the easy axis and $\vec{H}$. We typically observe multiple peaks: two large peaks that are each split and, often, small peaks to the right or left of the large peaks. Dispersive spectra show corresponding features (see Fig. 2 in Ref. [28]). The large peaks correspond to allowed transitions with $\Delta m \simeq \pm 1$. The splitting of these peaks arises from ligand conformational disorder [26]. Additional fine structure that some of these peaks exhibit [23] is not relevant to this study. We focus on the two small side peaks (marked $\star$ and $+$ in Fig. 2) that correspond roughly to $m = -4 \rightarrow m = 2$ ($\star$) and $m = 3 \rightarrow m = -4$ ($+$) (cf. Fig. 1, orange arrows). Compared with the allowed transitions, these forbidden transitions have markedly different dependences on $\theta_H$, confirming their different character.

Figure 3 shows the $B - \theta$ resonance positions (determined from the spectra in Fig. 2), where $\theta$ is the angle between the easy axis and the field $\vec{B}$ experienced by the molecules. Lines show the calculated resonance points for the transitions shown in Fig. 1, obtained by diagonalizing Eq. (1) using the parameters given below. Solid (dashed) curves indicate allowed (forbidden) transitions. The agreement between the calculated $B - \theta$ resonance positions and the experimental data is very good. In producing Fig. 3, we took into account that both the magnitude and direction of $\vec{B}$ changes with $\vec{H}$ due to intermolecular dipolar interactions, so that each spectrum in Fig. 2 produces a range of $\theta$ values in Fig. 3 [28]. Red and black curves show predicted resonance positions for the two conformational states (isomers) of the molecule, which have somewhat different anisotropy constants, determined by fitting [28]: $D = 15.13(4)$ GHz, $A = 0.136(2)$ GHz, and $C = 5.3(2)$ MHz (red), and $D = 15.55(4)$ GHz, $A = 0.138(2)$ MHz, $C = 6.45(3)$ MHz (black). $g$ factors were taken to be the same for both components and found to be $g_z = 2.157(7)$ and $g_x = g_y = 2.220(3)$. These numbers are in reasonable agreement with those found by others [19,20].

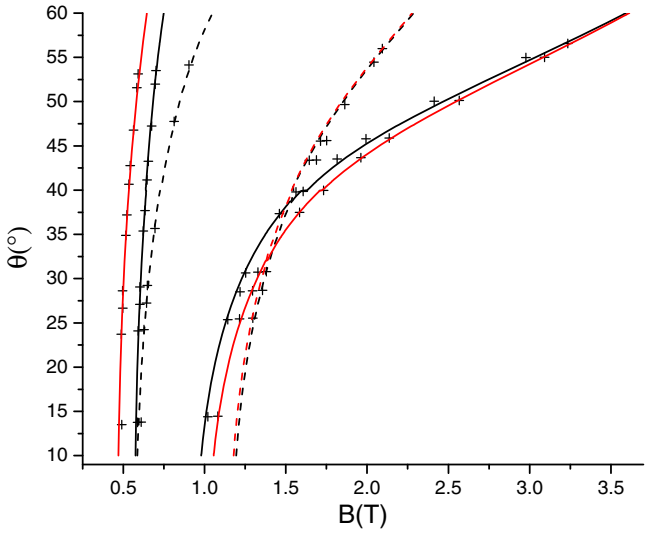


FIG. 3. Resonance positions in $B-\theta$ space. The points are the peak positions from Fig. 2 after correcting for the effects of dipole fields [28]. The lines are the results of simulations after fitting the observed spectra. Black and red correspond to different conformational states of the molecule with correspondingly different anisotropy constants. Solid curves indicate allowed transitions and dashed curves correspond to forbidden transitions. The small shift seen in the calculated results at ~40° arises from use of different samples at angles above and below this value and associated differences in the direction ($\phi$) of the transverse field in the samples' hard planes [28].

The forbidden transitions (orange arrows in Fig. 1) are observable because each occurs at a field near an anticrossing, where resonant tunneling takes place. Tunneling effects can be demonstrated by expanding the two energy eigenstates for each forbidden transition in the eigenbasis of $S_z$:

$$|E_j\rangle = \sum_m c_m^{(j)} |m\rangle. \quad (2)$$

Figures 4(a) and 4(b) show $|c_m|$ vs $m$ for the initial ($|i\rangle$) and final ($|f\rangle$) states involved in the $\star$ and $+$ transitions, respectively, at $\theta = 30°$ in the proximity of an anticrossing. For $\star$, $|i\rangle \approx |m=-4\rangle$, while $|f\rangle$ is a superposition of primarily $|m=2\rangle$, $|m=-3\rangle$, and $|m=1\rangle$. It is the proximity of the ESR transition to an anticrossing that produces a non-negligible amplitude of $|m=-3\rangle$ in $|f\rangle$ and thus a $\Delta m = 1$ transition matrix element between $|i\rangle$ and $|f\rangle$. The transition between states largely localized in separate wells constitutes a tunneling-assisted forbidden transition. Equivalently, the transition can be viewed as photon-induced tunneling in which the system transits between wells while absorbing the photon without acquiring enough energy to surmount the barrier. During this forbidden transition, the change of $m$ is nominally 6; indeed, a rigorous calculation yields a change in expectation value $|\Delta\langle S_z\rangle|$ as high as 6, indicating a large change in the spin's angular momentum with the absorption of a single photon [28].

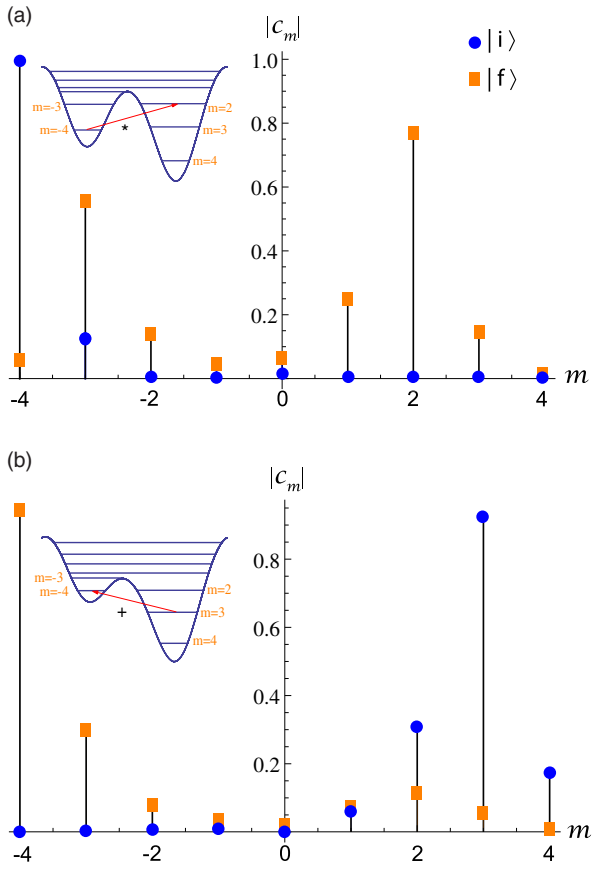


FIG. 4. Decomposition of eigenstates involved in the forbidden transitions in the $m$ basis [cf. Eq. (2)]. Values of $|c_m|$ were calculated by diagonalizing the spin Hamiltonian at the fields corresponding to the (a) $\star$ and (b) $+$ transitions, setting $\theta = 30°$. Blue circles (orange squares) indicate the values of $|c_m|$ for the lower (upper) state involved in each transition. Insets schematically show the double-well potentials for the associated transitions, marked with red arrows.

Similarly, the $+$ transition [Fig. 4(b)], involves $|i\rangle \approx |m=3\rangle$ and $|f\rangle$, a superposition of mostly $|m=-4\rangle$, $|m=-3\rangle$, and $|m=2\rangle$ states. This transition's proximity to an anticrossing here gives rise to a finite amplitude of $|m=2\rangle$ in $|f\rangle$ and a dipole matrix element with $|i\rangle$. For this transition, we calculate a maximum $|\Delta\langle S_z\rangle|$ of ~7 for experimentally relevant values of $B$ and $\theta$ [28].

The forbidden-transition peaks tend to become stronger when very close to the allowed transitions (Fig. 2), confirming the delocalization of $|f\rangle$ near the tunneling resonance field. A comparison of the experimental and simulated spectral intensity (Fig. 3 in Ref. [28]) shows good agreement, with the intensity growing near anticrossings or at large transverse fields, where tunneling is enhanced.

The peak linewidths for forbidden transitions tend to be significantly smaller than for allowed transitions (Fig. 2). The widths appear to roughly scale as $1/\Delta\langle S_z\rangle$. This suggests that these peaks are homogeneously broadened. Extracting $T_2$ from the widths, yields values ≈0.1–1 ns

(Fig. 4 in Ref. [28]), comparable to those found previously for $Ni_4$ [17]. Larger $T_2$ values are needed for realistic quantum information processing. Long $T_2$ times have been achieved in a variety of molecular magnets via dilution [4,6,8] to reduce dipole couplings; indeed, $Ni_4$ can be diluted by cocrystallizing it with the diamagnetic analog $Zn_4$ [29]. $T_2$ can also be enhanced by making use of "clock transitions," i.e., operating near an anticrossing, where $\partial f/\partial B = 0$ and decohering field fluctuations can only affect energies quadratically [3,12,16,31]. Nevertheless, the short $T_2$ we observe may be compensated by the high density of $Ni_4$ molecules in a crystal that can enhance the spin-photon coupling [32].

Independent of issues of coherence, the observed transitions have a distinctly "macroscopic" character, involving states with largely different values of $m$. Linear superpositions between such states are prototypical examples of macroscopic superposition states (*à la* Schrödinger's cat). Here we characterize the observed transitions $|i\rangle \to |f\rangle$ in terms of the linear superposition $|\psi\rangle = (|i\rangle + e^{i\eta}|f\rangle)/\sqrt{2}$ that can be generated through pulsed excitations, where $\eta$ typically depends on time. The macroscopicity of such states can be quantified using suitable measures, such as the quantum Fisher information (QFI) [33,34]

$$\mathcal{F}_\psi = \max_{X,\eta}(\langle\psi|X^2|\psi\rangle - \langle\psi|X|\psi\rangle^2). \tag{3}$$

Up to a constant (which we omit), QFI equals the variance of the operator $X = \sum_{i=1}^{N} \mathbf{n}_i \cdot \mathbf{s}_i$, where the $\mathbf{s}_i$ refers to the $i$th ionic spin of the molecule. $\mathcal{F}_\psi$ is maximized over all possible unit vectors $\mathbf{n}_i$ and with respect to the phase $\eta$. Here we consider states belonging to the maximal-spin multiplet ($S = 4$) of the $Ni_4$ molecule. One can show that in this case the maximum is always obtained with parallel vectors ($\mathbf{n}_i = \mathbf{n}, \ \forall i$).

We also determine the relative Fisher information,

$$D_{\mathrm{RFI}} = \frac{\mathcal{F}_\psi}{\frac{1}{2}(\mathcal{F}_i + \mathcal{F}_f)}, \tag{4}$$

in which each $\mathcal{F}$ is maximized independently. The above normalization allows one to single out the amount of quantum fluctuations in $|\psi\rangle$ that result from the linear superposition of the states $|i\rangle$ and $|f\rangle$. Figure 5 shows calculated oscillator strength (OS, transition matrix element squared) and $D_{\mathrm{RFI}}$ for the + transition of the black component between $|i\rangle = |E_2\rangle \approx |m = 3\rangle$ and $|f\rangle = |E_3\rangle$, the second and third lowest energy eigenstate, respectively, as a function of field. $\theta$ is adjusted to maintain the resonance condition between the radiation frequency and the transition, following the right dashed black curve in Fig. 3. At large fields, $|f\rangle \approx |m = 2\rangle$, the transition between these levels is allowed with a large OS and $D_{\mathrm{RFI}} \approx 1$. At low fields, $|f\rangle \approx |m = -4\rangle$ and the transition is more macroscopic ($D_{\mathrm{RFI}} \approx 3$)

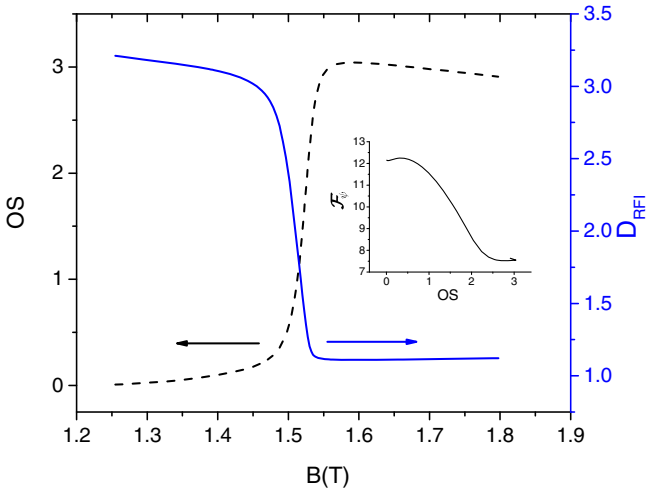


FIG. 5. Oscillator strength (OS) and $D_{\mathrm{RFI}}$ for one of the transitions studied as a function of field. Here $|i\rangle \approx |m = 3\rangle$ and $|f\rangle = |E_3\rangle$ are the second- and third-lowest energy eigenstates (cf. Fig. 1), respectively. As the field increases, the angle $\theta$ is adjusted to maintain resonance of the transition with the radiation frequency. For this pair of levels, the transition is forbidden (allowed) at small (large) fields with a crossover at the field of the anticrossing. The inset shows a parametric plot of $\mathcal{F}_\psi$ vs OS, illustrating how, near the anticrossing, one quantity rises as the other falls, but both can be substantial over some region. Similar calculations for the transition between $|E_2\rangle$ and $|E_4\rangle$, the second and fourth energy eigenstates, show complementary behavior [28].

and forbidden (OS small). Near the anticrossing, where states with very different values of $m$ hybridize, relatively large values of $D_{\mathrm{RFI}}$ can persist, while the oscillator strength remains finite. Interestingly, the behavior of $D_{\mathrm{RFI}}$ and $|\Delta\langle S_z\rangle|$ are qualitatively similar [28], indicating that $\Delta\langle S_z\rangle$ is a reasonable proxy for quantifying the macroscopicity of these transitions.

Our work demonstrates the important role tunneling can play in "opening up" forbidden transitions. In $Ni_4$, the relevant tunnel splittings for the transitions studied are relatively large (on the order of 1 GHz). As a consequence, $m$ is no longer a good quantum number near an anticrossing, enabling forbidden transitions with large $|\Delta\langle S_z\rangle|$ and macroscopicity. In addition, the large tunnel splittings allow tunneling effects to extend beyond the immediate vicinity of an anticrossing. In our experiments, the observed forbidden transitions lie slightly away from anticrossings, permitting *direct* single-photon transitions between states largely localized in opposite wells. When tunnel splittings are much smaller, one enters the regime of photon-assisted tunneling [35,36], where an allowed ESR transition is followed sequentially by tunneling between wells. Tunnel splittings can be enhanced by applying large transverse fields [17]. However, a field only acts as a perturbation when the Zeeman energy is small compared to the molecule's anisotropy energy. In the large-field regime,

the transitions become allowed and the macroscopicity of superposition states becomes suppressed. Furthermore, going beyond the perturbation regime undermines the advantages afforded by clock transitions. The tunnel splittings found intrinsically in $Ni_4$ are sufficient to observe forbidden transitions without the need of applying significant transverse fields to enhance tunneling.

We are indebted M. P. Sarachik for useful discussions and comments on the manuscript. We also thank D. I. Schuster and M. Foss-Feig for productive conversations. We are grateful to H. Xu for her assistance in some aspects of the numerical simulations. We thank C. Euvrard (Millitech Corp.) for technical help with some equipment, J. Kubasek for assistance in fabrication of the resonator, and N. Page for technical support of measurement equipment. Support for this work was provided by the U.S. National Science Foundation under Grant No. DMR-1310135, by the Italian Ministry of Education and Research through the FIRB project RBFR12RPD1 and RBFR13YKWX, and by the EU through the FP7 FET project MoQuaS (Contract No. 610449). J. R. F. acknowledges the support of the Amherst College Senior Sabbatical Fellowship Program, funded in part by the H. Axel Schupf '57 Fund for Intellectual Life. R. A. A. C. thanks CNPq for fellowship 202249/2012-3 that enabled his work at the University of Massachusetts Amherst.

*Current address: Department of Earth, Atmospheric and Planetary Sciences, Massachusetts Institute of Technology, Cambridge, Massachusetts 02139, USA.
†Instituto de Química, Universidade Federal do Rio de Janeiro, Rio de Janeiro, RJ, 21941-909 Brazil.
‡Corresponding author.
jrfriedman@amherst.edu

[1] D. I. Schuster, A. P. Sears, E. Ginossar, L. DiCarlo, L. Frunzio, J. J. L. Morton, H. Wu, G. A. D. Briggs, B. B. Buckley, D. D. Awschalom, and R. J. Schoelkopf, Phys. Rev. Lett. **105**, 140501 (2010).
[2] Y. Kubo, F. R. Ong, P. Bertet, D. Vion, V. Jacques, D. Zheng, A. Dréau, J.-F. Roch, A. Auffeves, F. Jelezko, J. Wrachtrup, M. F. Barthe, P. Bergonzo, and D. Esteve, Phys. Rev. Lett. **105**, 140502 (2010).
[3] G. Wolfowicz, A. M. Tyryshkin, R. E. George, H. Riemann, N. V. Abrosimov, P. Becker, H.-J. Pohl, M. L. W. Thewalt, S. A. Lyon, and J. J. L. Morton, Nat. Nanotechnol. **8**, 561 (2013).
[4] K. Bader, D. Dengler, S. Lenz, B. Endeward, S.-D. Jiang, P. Neugebauer, and J. van Slageren, Nat. Commun. **5**, 5304 (2014).
[5] M. N. Leuenberger and D. Loss, Nature (London) **410**, 789 (2001).
[6] A. Ardavan, O. Rival, J. J. L. Morton, S. J. Blundell, A. M. Tyryshkin, G. A. Timco, and R. E. P. Winpenny, Phys. Rev. Lett. **98**, 057201 (2007).
[7] C. J. Wedge, G. A. Timco, E. T. Spielberg, R. E. George, F. Tuna, S. Rigby, E. J. L. McInnes, R. E. P. Winpenny, S. J. Blundell, and A. Ardavan, Phys. Rev. Lett. **108**, 107204 (2012).
[8] C. Schlegel, J. van Slageren, M. Manoli, E. K. Brechin, and M. Dressel, Phys. Rev. Lett. **101**, 147203 (2008).
[9] L. Bogani and W. Wernsdorfer, Nat. Mater. **7**, 179 (2008).
[10] F. Troiani and M. Affronte, Chem. Soc. Rev. **40**, 3119 (2011).
[11] S. Ghosh, S. Datta, L. Friend, S. Cardona-Serra, A. Gaita-Ariño, E. Coronado, and S. Hill, Dalton Trans. **41**, 13697 (2012).
[12] M. Shiddiq, D. Komijani, Y. Duan, A. Gaita-Ariño, E. Coronado, and S. Hill, Nature (London) **531**, 348 (2016).
[13] J. R. Friedman and M. P. Sarachik, Ann. Rev. Cond. Mater. Phys. **1**, 109 (2010).
[14] J. R. Friedman, M. P. Sarachik, J. Tejada, and R. Ziolo, Phys. Rev. Lett. **76**, 3830 (1996).
[15] W. Wernsdorfer and R. Sessoli, Science **284**, 133 (1999).
[16] J. J. Bollinger, J. D. Prestage, W. M. Itano, and D. J. Wineland, Phys. Rev. Lett. **54**, 1000 (1985).
[17] E. del Barco, A. D. Kent, E. C. Yang, and D. N. Hendrickson, Phys. Rev. Lett. **93**, 157202 (2004).
[18] E.-C. Yang, W. Wernsdorfer, S. Hill, R. S. Edwards, M. Nakano, S. Maccagnano, L. N. Zakharov, A. L. Rheingold, G. Christou, and D. N. Hendrickson, Polyhedron **22**, 1727 (2003).
[19] R. S. Edwards, S. Maccagnano, E.-C. Yang, S. Hill, W. Wernsdorfer, D. Hendrickson, and G. Christou, J. Appl. Phys. **93**, 7807 (2003).
[20] C. Kirman, J. Lawrence, S. Hill, E.-C. Yang, and D. N. Hendrickson, J. Appl. Phys. **97**, 10M501 (2005).
[21] G. de Loubens, G. D. Chaves-O'Flynn, A. D. Kent, C. Ramsey, E. del Barco, C. Beedle, and D. N. Hendrickson, J. Appl. Phys. **101**, 09E104 (2007).
[22] G. de Loubens, A. D. Kent, V. Krymov, G. J. Gerfen, C. C. Beedle, and D. N. Hendrickson, J. Appl. Phys. **103**, 07B910 (2008).
[23] J. Lawrence, E.-C. Yang, R. Edwards, M. M. Olmstead, C. Ramsey, N. S. Dalal, P. K. Gantzel, S. Hill, and D. N. Hendrickson, Inorg. Chem. **47**, 1965 (2008).
[24] J. Lawrence, E.-C. Yang, D. N. Hendrickson, and S. Hill, Phys. Chem. Chem. Phys. **11**, 6743 (2009).
[25] E.-C. Yang, W. Wernsdorfer, L. N. Zakharov, Y. Karaki, A. Yamaguchi, R. M. Isidro, G.-D. Lu, S. A. Wilson, A. L. Rheingold, H. Ishimoto, and D. N. Hendrickson, Inorg. Chem. **45**, 529 (2006).
[26] D. N. Hendrickson, E.-C. Yang, R. M. Isidro, C. Kirman, J. Lawrence, R. S. Edwards, S. Hill, A. Yamaguchi, H. Ishimoto, W. Wernsdorfer, C. Ramsey, N. Dalal, and M. M. Olmstead, Polyhedron **24**, 2280 (2005).
[27] C. C. Beedle, J. J. Henderson, P.-C. Ho, T. Sayles, M. Nakano, J. R. O'Brien, K. J. Heroux, E. del Barco, M. B. Maple, and D. N. Hendrickson, Inorg. Chem. **49**, 5780 (2010).
[28] See Supplemental Material at http://link.aps.org/supplemental/10.1103/PhysRevLett.117.187202, which includes Refs. [25, 29, 30], for experimental methods, additional data, and details of data-analysis procedures.
[29] C. A. Collett, R. A. Allão Cassaro, and J. R. Friedman, arXiv:1609.09859.
[30] S. Stoll and A. Schweiger, J. Magn. Reson. **178**, 42 (2006).

[31] D. Vion, A. Aassime, A. Cottet, P. Joyez, H. Pothier, C. Urbina, D. Esteve, and M. H. Devoret, Science **296**, 886 (2002).
[32] A. W. Eddins, C. C. Beedle, D. N. Hendrickson, and J. R. Friedman, Phys. Rev. Lett. **112**, 120501 (2014).
[33] F. Fröwis and W. Dür, New J. Phys., **14**, 093039 (2012).
[34] F. Troiani and P. Zanardi, Phys. Rev. B **88**, 094413 (2013).
[35] L. Sorace, W. Wernsdorfer, C. Thirion, A.-L. Barra, M. Pacchioni, D. Mailly, and B. Barbara, Phys. Rev. B **68**, 220407 (2003).
[36] M. Bal, J. R. Friedman, W. Chen, M. T. Tuominen, C. C. Beedle, E. M. Rumberger, and D. N. Hendrickson, EPL **82**, 17005 (2008).